Chitosan/Arabic gum/ZnO bionanocomposite as a novel antibacterial agent

Mohsen Safaei[1), 2)] (ORCID ID: 0000-0003-3885-6640), **Mohammad Salmani Mobarakeh**[2)] (0000-0002-3272-4041), **Bahram Azizi**[3)] (0000-0001-8107-3284), **Ehsan Shoohanizad**[3)] (0000-0003-2596-8918), **Ling Shing Wong**[4)] (0000-0002-5869-0804), **Nafiseh Nikkerdar**[5), *)] (0000-0002-2477-1761)

DOI: https://doi.org/10.14314/polimery.2024.6.4

Abstract: The synthesis conditions of chitosan/Arabic gum /zinc oxide nanocomposite were optimized using the Taguchi method to obtain antibacterial properties. FT-IR, XRD, FESEM, EDX, TEM, UV/VIS and TGA techniques were used to characterize the nanocomposite. Nanocomposite C3 (1 mg/mL chitosan, 4.5 mg/mL Arabic gum and 8 mg/mL zinc oxide), C7 (3 mg/mL chitosan, 5.1 mg/mL Arabic gum and 8 mg/mL zinc oxide) and C9 (3 mg/mL chitosan, 4.5 mg/mL Arabic gum and 4 mg/mL zinc oxide) had the best antibacterial properties against *S. mutans*. TGA showed that ZnO improved the thermal stability of the nanocomposite. Such materials can be used as antibacterial agents.

Keywords: chitosan, Arabic gum, zinc oxide nanoparticles, process innovation, antimicrobial activity, Taguchi method.

Bionanokompozyt chitozan/guma arabska/ZnO jako nowy materiał antybakteryjny

Streszczenie: Przy użyciu metody Taguchi zoptymalizowano warunki syntezy nanokompozytu chitozan/guma arabska/tlenek cynku umożliwiające uzyskanie właściwości antybakteryjnych. Do scharakteryzowania nanokompozytu zastosowano techniki FT-IR, XRD, FESEM, EDX, TEM, UV/VIS i TGA. Nanokompozyt C3 (1 mg/mL chitozanu, 4,5 mg/mL gumy arabskiej i 8 mg/mL tlenku cynku), C7 (3 mg/mL chitozanu, 5,1 mg/mL gumy arabskiej i 8 mg/mL tlenku cynku) i C9 (3 mg/mL chitozanu, 4,5 mg/mL gumy arabskiej i 4 mg/mL tlenku cynku) miał najlepsze właściwości antybakteryjne wobec *S. mutans*. Metodą TGA wykazano, że ZnO poprawia stabilność termiczną nanokompozytu. Tego typu materiały mogą być stosowane jako środki antybakteryjne.

Słowa kluczowe: chitozan, guma arabska, ZnO, innowacja procesowa, aktywność antybakteryjna, metoda Taguchi.

Despite the constantly expanding knowledge in all fields of medicine, bacterial infections remain a serious and growing medical problem. Most of the current antimicrobial agents have been used for more than several decades. As a result, current antimicrobial agents face a real risk of losing their efficacy against bacteria and treating bacterial infections. According to the statement of the UN General Assembly in 2016, it is estimated that if bacterial resistance continues to increase at the current rate, incurable infections caused by bacteria will become the leading cause of death by 2050 [1, 2].

Infections caused by dental biofilms are among those resistant to common antimicrobial agents. The main components of the matrix in dental caries-related oral biofilms are exopolysaccharides, especially glucans derived from *S. mutans*. The cariogenic *S. mutans* specifically metabolizes dietary sucrose into insoluble exopolysaccharides, which increases the adhesion and cohesion of bacteria and their accumulation on the tooth surface, causing the formation of an acidic biofilm and caries. Therefore, *S. mutans* has been considered a key modulator in caries development due to its vital capacity to synthesize and distribute exopolysaccharides in dental biofilms. Currently, more attention is focused on the development of suitable compounds to target *S. mutans*, thus control its pathological conditions [3]. Nanomaterials have been

[1)] Division of Dental Biomaterials, School of Dentistry, Kermanshah University of Medical Sciences, Kermanshah 54658, Iran.

[2)] Advanced Dental Science and Technology Research Center, School of Dentistry, Kermanshah University of Medical Sciences, Kermanshah 38647, Iran.

[3)] Department of Oral and Maxillofacial Surgery, School of Dentistry, Kermanshah University of Medical Sciences, Kermanshah 54658, Iran.

[4)] Faculty of Health and Life Sciences, INTI International University, Nilai 71800, Malaysia.

[5)] Department of Oral and Maxillofacial Radiology, School of Dentistry, Kermanshah University of Medical Sciences, Kermanshah 54658, Iran.

[*)] Author for correspondence: nikkerdarnafiseh@gmail.com

considered as new antimicrobial agents for the treatment and prevention of infectious diseases with favorable effectiveness. The most common nanostructured antibacterial materials include metallic or non-metallic nanoparticles (silver, gold, copper, bismuth, selenium) and metal oxide nanoparticles such as ZnO, TiO_2, CaO, MgO, Fe_2O_3 or Al_2O_3. Most of these nanostructured materials show their antibacterial effects through non-specific activity, which can limit the development of bacterial resistance [3–5]. In recent years, research has focused on the synthesis of metal oxides or metal nanoparticles using polysaccharide gums as stabilizing agents against nanoparticle aggregation. These synthesized biocomposites can be used in different fields as biocarriers or as antimicrobial agents [6].

Zinc oxide nanoparticles are compatible with skin and human body cells, so they can be used as a coating for medical devices and textiles that are in contact with the human body [7]. One of the main problems of metal nanoparticles is their instability and agglomeration. Hence, identifying a new class of biocompatible materials that can be combined with ZnO is necessary to develop safe and cost-effective biomaterials with significant antimicrobial activity against pathogenic bacteria and fungi [8].

Chitosan is a polysaccharide obtained from the deacetylation of chitin; a natural polymer found in the exoskeleton of crustaceans. Chitin is insoluble in aqueous solutions, while chitosan is soluble in acidic media. Chitosan has been reported to have moisturizing, antioxidant, anti-inflammatory and antimicrobial properties. Arabic gum is a natural polysaccharide obtained from the acacia tree, which is an amphiphilic branched polysaccharide that has good emulsifying properties and low viscosity and is used in various applications, including food, textile, biomedical, cosmetic, and pharmaceutical industries [9, 10].

In this study, a novel chitosan-based nanocomposite using Arabic gum and zinc oxide nanoparticles with antibacterial activity against *S. mutans* was obtained using the Taguchi method. The conditions for the synthesis of the nanocomposite with the highest antibacterial activity were optimized. This composite may be particularly useful in health-related applications where the control of bacterial growth is crucial. It may find applications in various fields, including tissue engineering, antibacterial packaging, biomedical and dental applications.

EXPERIMENTAL PART

Materials

Zinc oxide nanoparticles, zinc chloride, sodium hydroxide potassium hydroxide, chitosan biopolymer (with 92% degree of deacetylation, molecular weight (M_w) of 130 kDa), Arabic gum (trade name Gum Arabic, density of 1.4 g/cm^3) were purchased from Merck (Darmstadt, Germany). All the reagents were over 99 wt% purity.

Synthesis of zinc oxide nanoparticles

0.83 g of zinc chloride salt, 1.19 g of sodium hydroxide, and 1.1 g of potassium hydroxide were mixed. Next, reagents were put in an oven set to 220°C for 45 min. The finished product was centrifuged after being cooled to room temperature and rinsed three times with hot distilled water to remove contaminants. A white powder of zinc oxide nanoparticles was created by baking the precipitate for two hours at 100°C [11].

Synthesis of chitosan/Arabic gum/ZnO nanocomposites

Qulitek-4 software was used to calculate and identify the ideal circumstances for the synthesis of nanocomposites with the highest antibacterial activity. Nine tests with various ratios of zinc oxide nanoparticles, chitosan biopolymer and Arabic gum biopolymer were obtained using Taguchi's methodology. Using the *in-situ* approach, concentrations of 1.5, 3, and 4.5 mg/mL of Arabic gum, and 1, 2, and 3 mg/mL of chitosan and 2, 4, and 8 mg/mL of zinc oxide nanoparticles were used to examine the antibacterial characteristics of the synthesized nanocomposite (Table 1).

For this purpose, according to the experiments designed by the Taguchi method, solutions with different concentrations of chitosan, Arabic gum, and zinc oxide nanoparticles were stirred in separate containers for one hour and each was sonicated for 15 min until the solution was dissolved. Containers containing chitosan solution were placed on a magnetic stirrer and Arabic gum solutions and zinc oxide nanoparticles were added to them drop by drop at the same time. The final solutions were stirred using a magnetic stirrer for one hour and then sonicated for 15 min until the nanocomposites were formed. To prepare the powder of nanocomposites, the resulting solutions were dried in an oven at 60°C for 24 hours [12].

T a b l e 1. Taguchi experimental data on the synthesis of chitosan/Arabic gum/ZnO nanocomposite with the highest antibacterial activity

Sample	Chitosan mg/mL	Arabic gum mg/mL	ZnO mg/mL
C1	1	1.5	2
C2	1	3	4
C3	1	4.5	8
C4	2	1.5	4
C5	2	3	8
C6	2	4.5	2
C7	3	1.5	8
C8	3	3	2
C9	3	4.5	4

Antibacterial activity

S. mutans (ATCC 35668) was employed to evaluate the chitosan/Arabic gum/zinc oxide nanocomposite's antibacterial efficacy against biofilm. This bacterium was acquired from an Iranian industrial microorganism collection facility. *S. mutans* was cultivated on brain and heart extract agar media for 24 hours to create a single colony. Then, 0.5 McFarland worth of bacterial suspension was made. A bacterial biofilm was created by incubating the bacterial suspension in an aerobic environment for 72 hours at 37°C. New brain and heart extract containing 2 wt% sucrose and 1 wt% mannose was added to the culture medium daily. After biofilm formation, planktonic *S. mutans* was eliminated by three PBS washes. The Taguchi method's nanocomposite designed nanocomposite was then applied to each well of the plate, and it was incubated for 24 hours. After 24 hours of incubation at 37°C, the cells isolated from the well wall were collected to count the number of living cells in the biofilms. After being washed three times, the cells that still adhered to the well's wall were suspended in 1 mL of PBS buffer. The resulting suspension was then homogenized for 2 min using a vortex shaker. The bacterial sample was diluted ten times to perform the colony forming unit (CFU) test which were cultivated from brain and heart extract for 24 hours at 37°C on agar plates. After heating, colonies were counted, and their average of their numbers over nine tests was determined. Three repetitions of each experiment were performed [13, 14].

Methods

Fourier transform infrared spectroscopy (FT-IR) (ThermoFisher Scientific, Waltham, USA) was used to analyze the chemical structure. The spectra were recorded using at least 32 scans with 2 cm^{-1} resolution, in the spectral range of 4000-400 cm^{-1}, using KBr pellets technique. Crystal structure was determined by X-ray diffraction spectroscopy (XRD) using Philips X' Pert (Amsterdam, the Netherlands) diffractometer with monochromatic CuK α radiation (γ = 0.154056 nm) at 40 kV and 30 mA. Miller indices of different planes namely (hkl), (100), (002), (101), (102), (110), (103), (112) and (201) at specific angles, namely 2θ, 32, 35, 36, 48, 57, 63, 68 and 70 degrees were calculated in accordance with established academic protocols [15]. Morphology analyses were carried out using field emission scanning electron microscopy (FESEM) (MIRA3, TESCAN, Brno, Czech Republic), X-ray energy diffraction spectroscopy (EDX) (MIRA III model SAMX detector/France), element distribution map (Map) with SAMX detector (MIRA2, TESCAN, Brno, Czech Republic), and transmission electron microscopy (TEM) (TEM Philips EM208S, Amsterdam, The Netherlands). UV/VIS spectroscopy (Shimadzu UV- 160 A, Tokyo, Japan) was used to analyze optical properties. Thermal properties were determined using thermogravimetric analyzer, and differential scanning calorimeter (TGA-DSC) (TA Q600, TA Instruments, New Castle, Great Britain) in an argon atmosphere at heating rate of 20°C/min, from 25 to 800°C.

RESULTS AND DISCUSSION

Antibacterial activity

The optimal conditions for the synthesis of chitosan/Arabic gum/zinc oxide nanocomposite with the highest antibacterial activity were determined using the Taguchi method. Then, the effect of the nanocomposite obtained under different conditions on the viability of *S. mutans* was evaluated. The results show that samples C3 (1 mg/mL of chitosan, 4.5 mg/mL of Arabic gum, and 8 mg/mL of zinc oxide), C7 (3 mg/mL of chitosan, 5.1 mg/mL of Arabic gum, and 8 mg/mL of zinc oxide), and C9 (3 mg/mL of chitosan, 4.5 mg/mL of Arabic gum, and 4 mg/mL of zinc oxide) showed the strongest antibacterial efficacy against biofilm containing *S. mutans*, as shown in Fig. 1.

The way of killing bacteria can be different, depending on the mechanism. The most common is the generation of reactive oxygen species (ROS), which leads to the disruption of the bacterial cell wall by inducing oxidative stress, causing enzyme inhibition, changes in gene expression and protein inactivation [16, 17]. It is known that ZnO nanoparticles attach to the bacterial surface, causing disruption of the cell membrane, which leads to the leakage of cytoplasmic components and cell death [18] through the production of ROS, especially hydrogen peroxide [19].

Figure 2 depicts the impact of chitosan, Arabic gum, and zinc oxide factors on the survivability of *S. mutans*. The viability of the bacteria was most significantly influenced by these factors at the third level.

Notably, chitosan at the first level and Arabic gum at the third level exhibited a robust interaction effect, resulting in a 22.13% reduction in the survival rate of *S. mutans* (Fig. 3). Additionally, chitosan at the first level and zinc oxide at the third level demonstrated a specific interaction, causing a 19.67% decrease in the survival rate of *S. mutans*. Finally, the third level showed the lowest level of interaction intensity index, which was 9.28% for Arabic

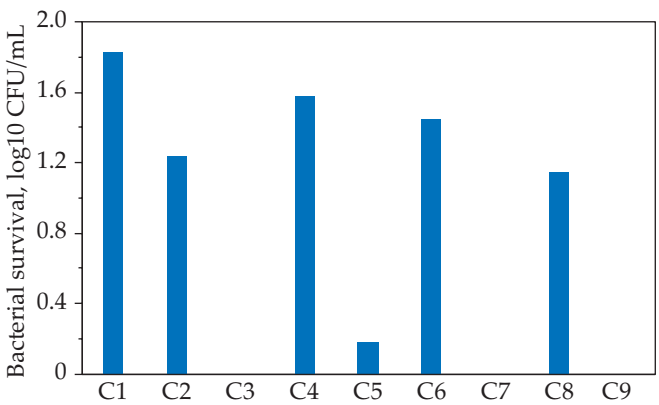

Fig. 1. Survival rate of *S. mutans* of nanocomposites

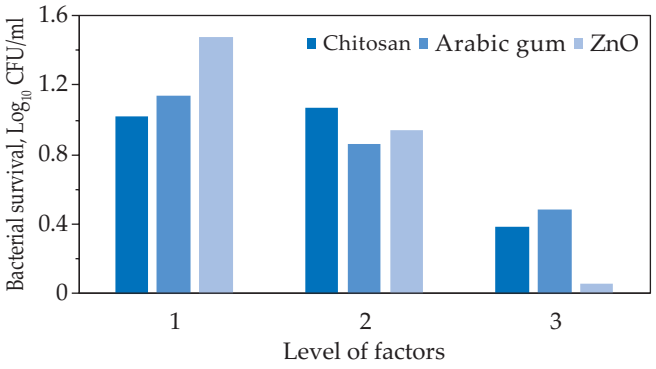

Fig. 2. The effect of chitosan, Arabic gum, and ZnO factors on the survival rate of *S. mutans*

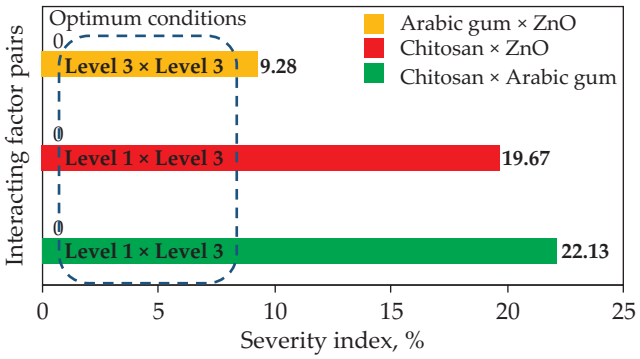

Fig. 3. Effect of the tested factors on the inhibition of *S. mutans* biofilm growth

T a b l e 2. Factors influencing the limitation of *S. mutans* biofilm growth

Factors	DOF*)	Sum of squares	Variance	F-ratio, F	Pure sum	Percent %
Chitosan	2	0.88	0.44	8.09	0.77	16.45
Arabic gum	2	0.64	0.32	5.91	0.54	11.38
ZnO	2	3.07	1.53	28.12	2.96	62.90

*) DOF – degree of freedom

gum and zinc oxide. The influence of parameters on *S. mutans* survival is presented in Table 2.

It can be concluded that zinc oxide had the greatest effect on the viability of *S. mutans* (62.9%). The effect of chitosan was 16.45%, and Arabic gum 11.38%. Table 3 summarizes the most favorable conditions for obtaining chitosan/Arabic gum/zinc oxide nanocomposite with the highest antibacterial activity.

T a b l e 3. Optimal conditions for the synthesis of chitosan/Arabic gum/ZnO nanocomposites with the highest antibacterial activity

Factors	Level	Contribution
Chitosan	3	0.44
Arabic gum	3	0.34
ZnO	3	0.77
Total contribution from all factors		1.55
Current grand average of performance		0.82
Bacterial survival at optimal conditions		-0.73

The present study reveals that zinc oxide showed the greatest effect on the survival rate of *S. mutans*, while Arabic gum had the least effect. Interestingly, chitosan had an intermediate effect, close to Arabic gum. Furthermore, the third level was found to be the optimum level for all the three variables, namely chitosan, Arabic gum, and zinc oxide. In the case of nanocomposites C3, C7 and C9, biocidal properties were obtained.

Chemical structure

The FT-IR spectra of chitosan, Arabic gum, zinc oxide and nanocomposite are shown in Fig. 4. In the FT-IR

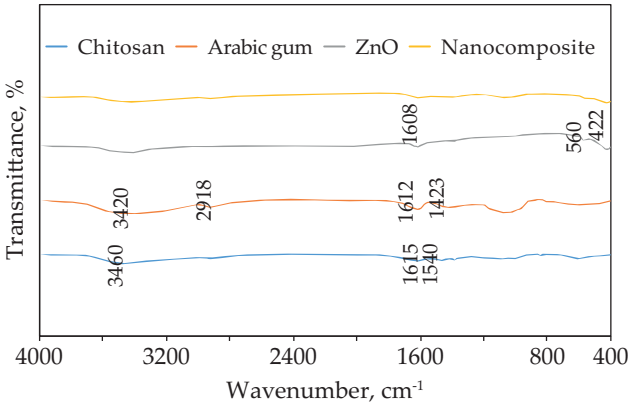

Fig. 4. FT-IR spectra of chitosan, Arabic gum, ZnO and chitosan/Arabic gum/ZnO nanocomposite

spectrum of chitosan, a peak at 1615 cm^{-1} was observed, which corresponds to the characteristic $CONH_2$ group. Moreover, the stretching oscillation of the combined peaks of NH_2 and OH groups was found to occur at 3460 cm^{-1}. The appearance of the peak at 1540 cm^{-1} indicates the gamma bending oscillation of NH_2 and is related to the high degree of deacetylation observed in chitosan. The higher intensity of the peak at 3460 cm^{-1} could be attributed to the presence of nanometric chitosan particles and is additionally associated with a considerable number of hydrogen bonds. Moreover, the band with a subdued intensity corresponding to $CONH_2$ at 1615 cm^{-1} and the band (NH_2) at 1540 cm^{-1} indicate the purity of chitosan [20].

Arabic gum spectrum shows a wide-ranging absorption band at 3000–3500 cm^{-1} (with a peak at 3420 cm^{-1}), manifesting the existence of OH groups interlinked to H, akin to the absorption band of the amine group in the region. The CH groups are associated with the bands

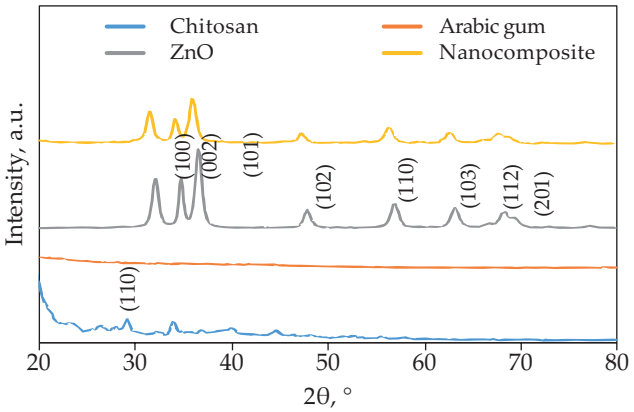

Fig. 5. XRD patterns of chitosan, Arabic gum, ZnO and the nanocomposite

located at the wavenumbers of 2918 cm^{-1} and 1612 cm^{-1}, which correspond to the deformational motion. The polysaccharide molecules exhibit significant and robust vibration modes, which are primarily allocated within the spectrum of 1000 to 1100 cm^{-1}.

The band observed in the range of 1200–1400 cm^{-1} is related to the fluctuations of C-O and C-O-C bonds and is characteristic of naturally occurring polysaccharides. The vibrational modes produced by the pyranose rings present in the polysaccharide give rise to the bands occurring in the range of 750–900 cm^{-1}. The low peak intensity band at 1423 cm^{-1} indicates the vibration of the C-O bond. The Arabic gum molecule's carboxylate groups exhibit a distinct peak in the range of 1700–1540 cm^{-1}, which can be attributed to the presence of C=O stretching and N-H bending deformations. The bands originating from glycoprotein groups overlap with the bands of polysaccharide groups [21, 22].

In the FT-IR spectrum of zinc oxide nanoparticles, a broad absorption in the region of 3000–3600 cm^{-1} was observed, which was attributed to the O-H stretching caused by residual alcohols, water, and Zn-OH bond. The bending vibration of H-OH bond associated with zinc oxide nanoparticles was observed at 1608 cm^{-1}. The most prominent and broad absorption band occurring at 422 cm^{-1} could be attributed to the vibrational stretching of oxygen and zinc. Moreover, the pure zinc oxide nanoparticle samples showed Zn-O stretching bands at 422 and 560 cm^{-1}, as indicated in the previous studies [23].

The FT-IR spectrum of the nanocomposite shows characteristic peaks originating from the polymer components (chitosan, Arabic gum) and zinc oxide nanoparticles. However, the change in the intensity of these peaks indicates strong interactions between the components, thus confirming the formation of the nanocomposite.

Crystal structure

The crystal structure and composition of examined samples were determined using the X-ray diffraction spectroscopy, and the spectra are shown in Fig. 5. The present study involves the calculation of Miller indices of different planes namely (hkl), (100), (002), (101), (102), (110), (103), (112) and (201) at specific angles, namely 2θ, 32, 35, 36, 48, 57, 63, 68 and 70 degrees [15]. These calculations were performed in accordance with established academic protocols and the obtained data were analyzed in a rigorous and systematic manner. Furthermore, the Miller index of the plane (hkl), (110) corresponding to the angle 2θ was determined to be 20 degrees [24]. Arabic gum was found to have a semi-crystalline phase based on the results obtained from the X-ray diffraction [12]. The hexagonal crystal structure of the zincite phase was identified by the X-ray diffraction pattern of the zinc oxide nanoparticles. The nanocomposite X-ray diffraction pattern showed a change in peak intensity, broadening or disappearance of peaks, as well as shift of the peaks to the left or right of the spectrum compared to the X-ray diffraction patterns of the components.

Morphology

Fig. 6 shows field emission scanning electron microscope (FESEM) images of chitosan, zinc oxide nanoparticles, and chitosan/Arabic gum/zinc oxide nanocomposite. The interpenetrated network structure can be observed

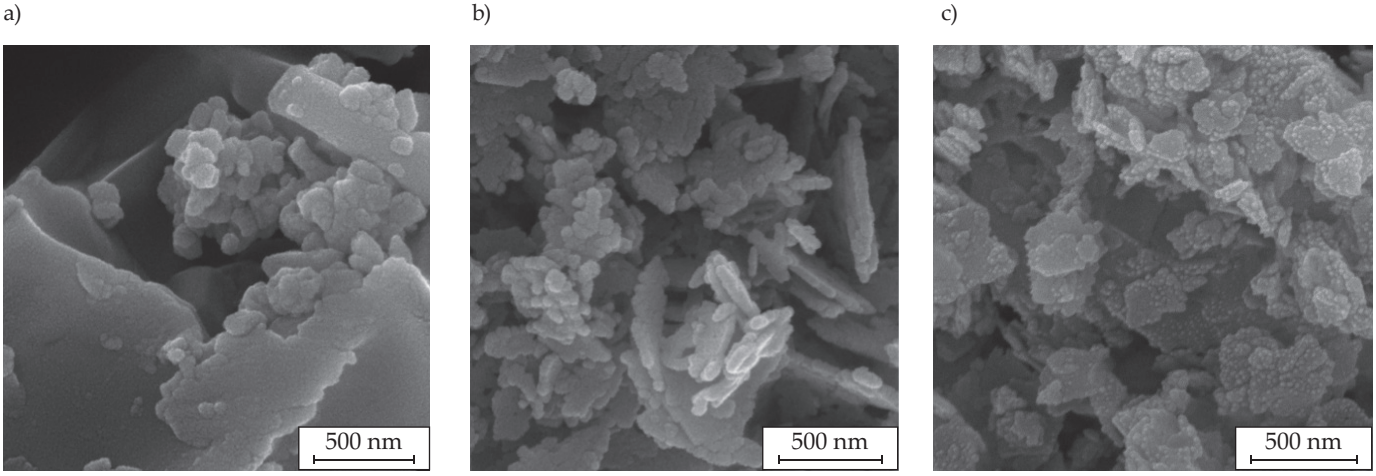

Fig. 6. FESEM images: a) chitosan, b) ZnO, c) chitosan/Arabic gum/ZnO nanocomposite

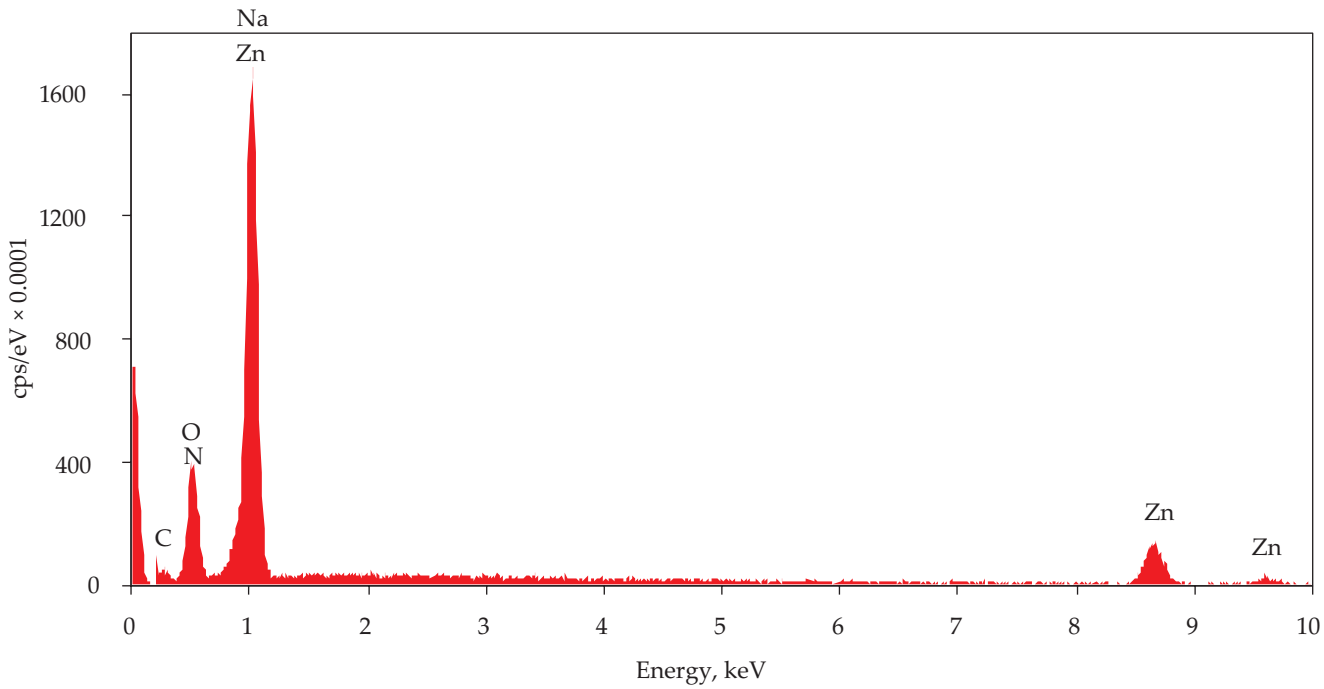

Fig. 7. EDS spectrum of chitosan/Arabic gum/ZnO nanocomposite

in FESEM images. In addition, the release of zinc oxide nanoparticles, nanoparticle clusters, and the appearance of larger particles due to the significant surface-to-volume ratio can be observed. By comparing the field emission scanning electron microscope images of the samples, it was possible to confirm the incorporation of zinc oxide nanoparticles as reinforcing agents into the chitosan and Arabic gum polymer matrix.

The results of energy-dispersive X-ray spectroscopy (EDS) for chitosan/Arabic gum/zinc oxide composite is shown in Fig. 7.

The components were identified to encompass carbon (10.82 wt%), nitrogen (3.55 wt%), oxygen (22.70 wt%), sodium (20.55 wt%), and zinc (42.39 wt%). The formation of the studied nanocomposite has been validated. Fig. 8 presents the distribution map of the elements on the sur-

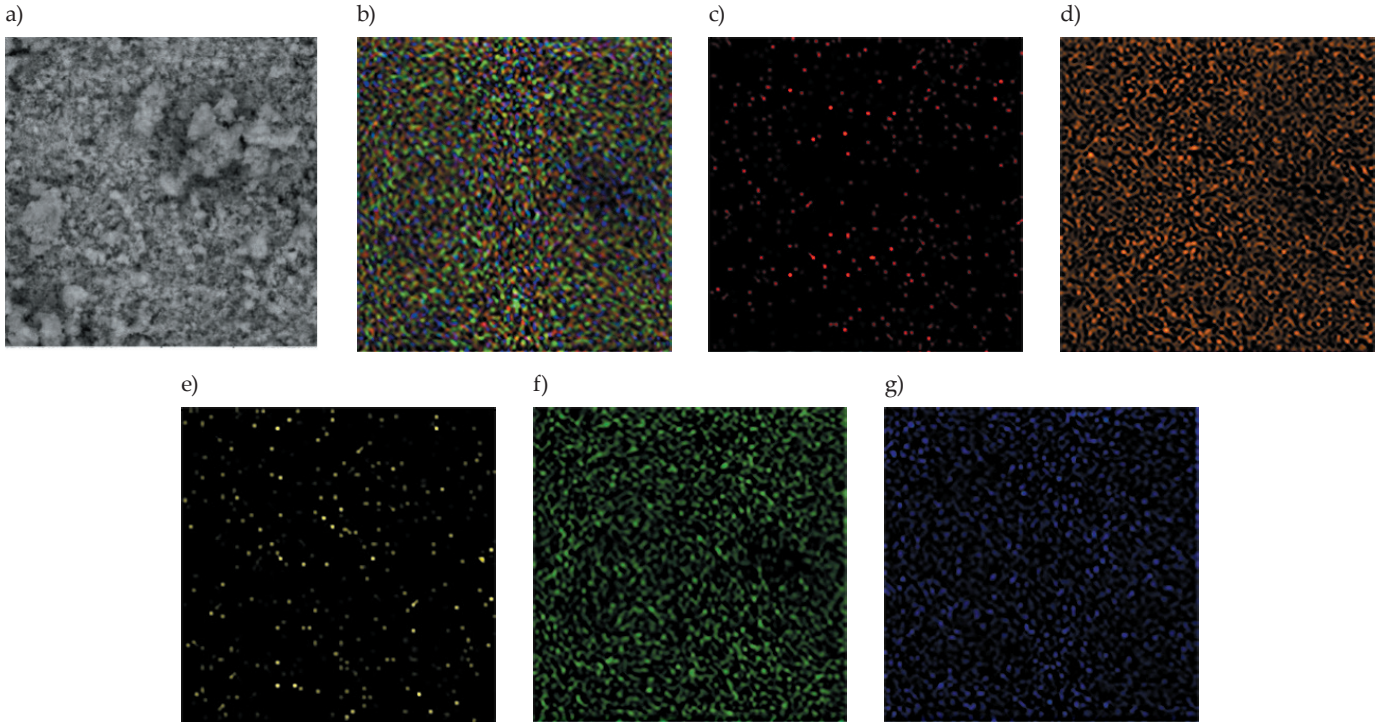

Fig. 8. Dispersion map: a) composition components on the surface of the nanocomposite, b) all elements, c) carbon, d) sodium e) nitrogen, f) oxygen, g) zinc

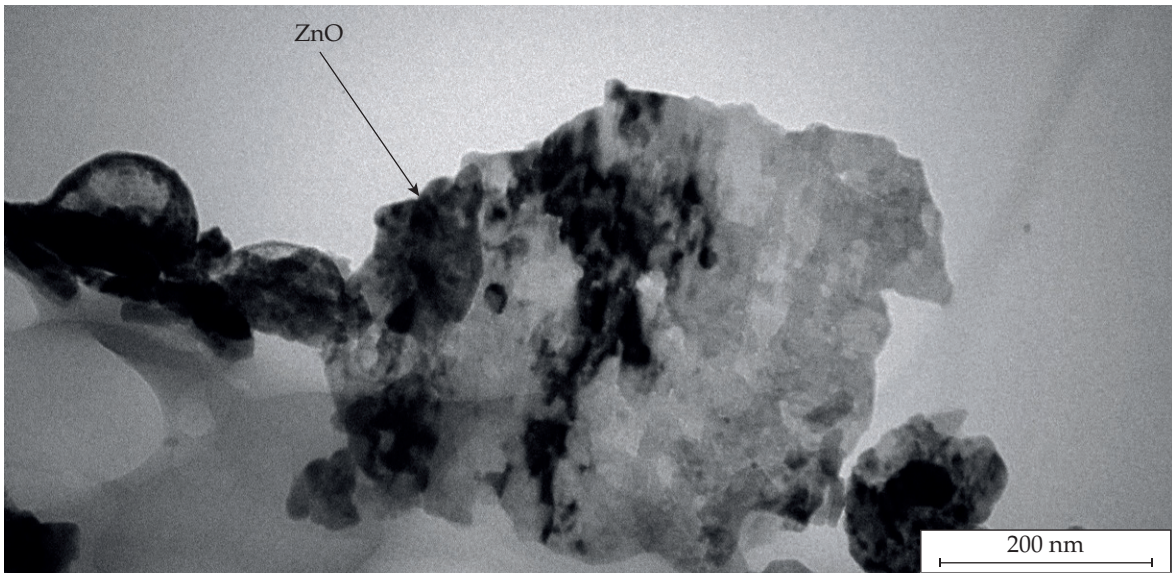

Fig. 9. TEM image of the nanocomposite

face of the chitosan/Arabic gum/zinc oxide nanocomposite. The synthesized nanocomposite has exhibited a uniform distribution of carbon, nitrogen, oxygen, sodium, and zinc elements in its overall composition, thus confirming the formation of the nanocomposite.

Fig. 9 shows the TEM image of nanocomposite confirming that zinc oxide nanoparticles are randomly dispersed and embedded in the chitosan and Arabic gum polymer matrix. This can be clearly observed as dark areas in the image.

Optical properties

UV/VIS spectroscopy in the range of 200–800 nm was used to study the optical properties of the chitosan/Arabic gum/zinc oxide nanocomposite and its components (Fig.10). The morphology of nanoparticles and their dimensions may affect their light absorption characteristics. A characteristic absorption band at 208 nm was detected in the spectrum of chitosan (Fig. 10a). Moreover, an absorption band at 195 nm was identified in the spectrum of Arabic gum (Fig. 10b). The absorption rate of the synthesized ZnO nanoparticles depends on factors, such as the energy band, oxygen content, surface roughness, and impurity centers. In the case of ZnO nanoparticles, an absorption peak at about 370 nm is visible [25, 26]. The observed differences in the spectra of the nanocomposite and its components confirmed the composition of the chitosan/Arabic gum /zinc oxide nanocomposite. In particular, the spectrum of the nanocomposite (Fig. 10d) showed the occurrence of two absorption peaks in the ranges of 195 and 372 nm. The occurrence of a double peak indicates an alternative size dispersion of the nanocomposite [22].

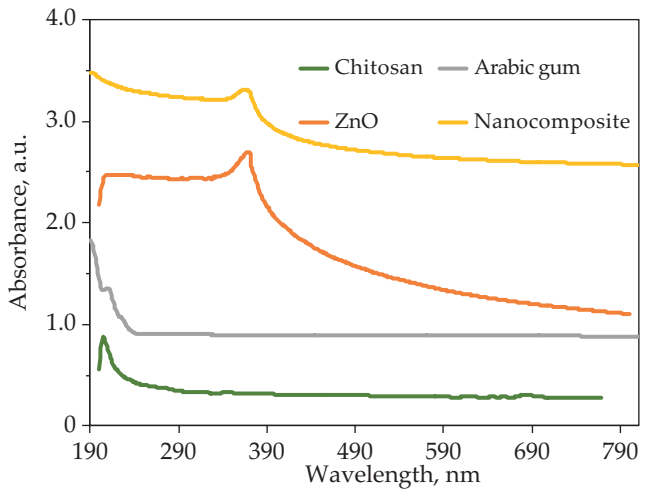

Fig. 10. UV/VIS spectra of chitosan, Arabic gum, ZnO and chitosan/Arabic gum/ZnO nanocomposite

Thermal properties

Thermogravimetric analysis (TGA) was used to determine the thermal properties of chitosan and nanocomposite, as shown in Fig. 11. Figure 11a shows that the thermal decomposition of chitosan occurred in two separate stages.

The first stage occurs in the temperature range from 40 to 145°C and results in 69% weight loss, due to water desorption enclosed in chitosan. The second stage is in the temperature range from 145 to 453°C and reaches a peak temperature of 260°C. The increase in temperature can be attributed to the degradation and decomposition of hydroxyl groups along the polymer chains and the dehydration of chitosan segments. Thermal decomposition of chitosan is accompanied by a significant degradation process at about 350°C, which ends with the combustion of the remaining substances. Moreover, the total weight loss at 450°C is as much as 30%. In the temperature range from 453 to 800°C, thermal decomposition of impurities occurs [27]. The thermograms derived

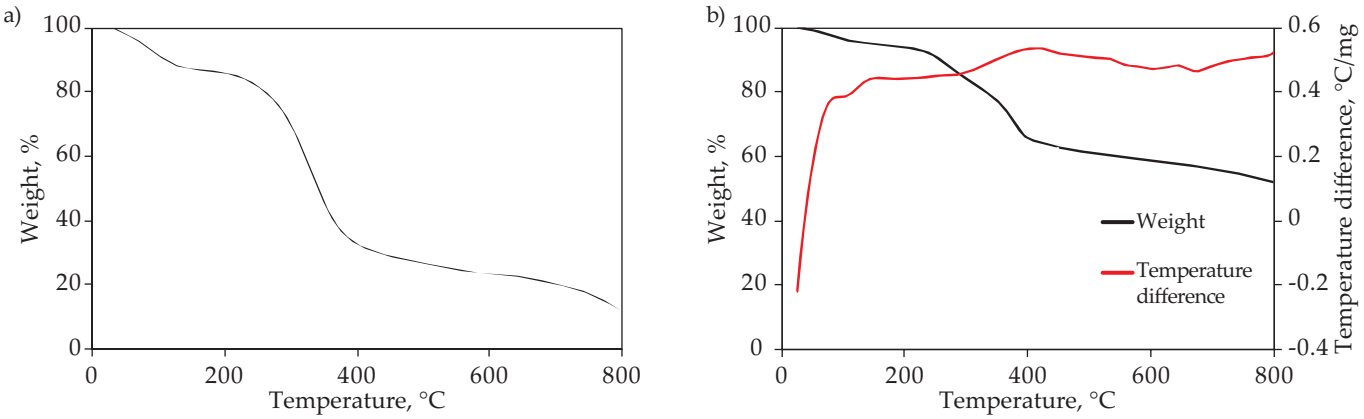

Fig. 11. Thermogravimetric curves: a) chitosan, b) nanocomposite

from the chitosan/Arabic gum/zinc oxide nanocomposite showed the three primary regions of weight loss. The obtained samples exhibited an initial weight loss in the temperature range of 40-130°C, due to the disintegration and volatilization of feeble linkages of physical dampness that were adsorbed on the sample's surface. The second weight loss was observed in the temperature range of 130–400°C and was caused by thermal decomposition of chitosan. The primary cause of this phenomenon is the presence of ceramic zinc oxide nanoparticles. The third stage of weight loss is observed in the temperature range of 500-800°C. Both samples exhibited a weight loss of approximately 10% at a temperature of 100°C. A significant reduction in weight loss was noted in the temperature range of 250-350°C. The initial degradation temperature of the nanocomposite was shown to be higher than that of chitosan. This observation indicates that thermal stability of chitosan and Arabic gum is improved by the addition of zinc oxide nanoparticles [24, 28, 29].

CONCLUSIONS

Taguchi method was used to obtain the optimal conditions for the synthesis and improvement of the antibacterial properties of chitosan/Arabic gum/zinc oxide nanocomposite. The nanocomposite synthesized under optimal conditions predicted by the software can completely (-0.73 Log_{10} CFU/mL) prevent the activity of *S. mutans* and stop their growth and survival (zinc oxide with the highest efficacy, chitosan with a medium effect and Arabic gum with the lowest effect). This nanocomposite can be used as an antimicrobial and antibiofilm agent in various fields of biology, medicine, and dentistry.

ACKNOWLEDGMENTS

The authors gratefully acknowledge the Research Council of Kermanshah University of Medical Sciences for the financial support under grant number 990292.

Authors contribution

M.S. – research concept, methodology, writing-original draft, project administration; M.S.M. – investigation, software, formal analysis; B.A. – visualization, resources; E.S. – visualization, writing - review and editing; L.S.W. – visualization, funding acquisition, writing; N.N. – research concept, supervision, validation, writing-review and editing.

Funding

The authors gratefully acknowledge the Research Council of Kermanshah University of Medical Sciences for the financial support under grant number 990292.

Conflict of interest

The authors declare no conflict of interest.

REFERENCES

[1] Taran M., Etemadi S., Safaei M.: *Journal of Applied Polymer Science* **2017**, *134(12)*, 44613. https://doi.org/10.1002/app.44613

[2] Hochvaldová L., Večeřová R., Kolář M. *et al.*: *Nanotechnology Reviews* **2022**, *11*, 1115. https://doi.org/10.1515/ntrev-2022-0059

[3] Mao M., Zhang W., Huang Z. *et al.*: *International Journal of Nanomedicine* **2021**, *16*, 7727. https://doi.org/10.2147/IJN.S303521

[4] Toprakcioglu Z., Wiita E.G., Jayaram A.K. *et al.*: *ACS Applied Materials and Interfaces* **2023**, *15(8)*, 10452. https://doi.org/10.1021/acsami.2c21013

[5] Han C., Romero N., Fischer S. *et al.*: *Nanotechnology Reviews* **2017**, *6(5)*, 383. https://doi.org/10.1515/ntrev-2016-0054

[6] Chelu M., Moreno J. C., Atkinson I. *et al.*: *International Journal of Biological Macromolecules* **2022**, *211*, 410.

https://doi.org/10.1016/j.ijbiomac.2022.05.070
[7] Nikdel M., Rajabinejad H., Yaghoubi H. *et al*.: *ECS Journal of Solid-State Science and Technology* **2021**, *10(5)*, 057003. https://doi.org/10.1149/2162-8777/abfc26
[8] Visnuvinayagam S., Murthy L.N., Parvathy U. *et al*.: *FEMS Microbiology Letters* **2021**, *368*, 210. https://doi.org/10.1093/femsle/fnaa210
[9] Sharkawy A., Casimiro F.M., Barreiro M.F. *et al*.: *International Journal of Biological Macromolecules* **2020**, *147*, 150. https://doi.org/10.1016/j.ijbiomac.2020.01.057
[10] Sharkawy A., Barreiro M.F., Rodrigues A.E.: *Carbohydrate Polymers* **2019**, *224*, 115190. https://doi.org/10.1016/j.carbpol.2019.115190
[11] Ghorbani F., Gorji P., Mobarakeh S.M. *et al*.: *Journal of Nanomaterials* **2022**, 7255181. https://doi.org/10.1155/2022/7255181
[12] Safaei M., Taran M., Imani M.M. *et al*.: *Polish Journal of Chemical Technology* **2019**, *21(4)*, 116. https://doi.org/10.2478/pjct-2019-0047
[13] Imani M.M., Kiani M., Rezaei F. *et al*.: *Ceramics International* **2021**, *47(12)*, 33398. https://doi.org/10.1016/j.ceramint.2021.08.246
[14] Safaei M., Moghadam A.: *Materials Today Communications* **2022**, *31*, 103698. https://doi.org/10.1016/j.mtcomm.2022.103698
[15] Getie S., Belay A., Chandra Reddy A.R. *et al*.: *Journal of Nanomedicine and Nanotechnology* **2017**, *8*, 004. http://dx.doi.org/10.4172/2157-7439.S7-001
[16] Gao W., Zhang L.: *Nature Reviews Microbiology* **2021**, *19*, 5. https://doi.org/10.1038/s41579-020-00469-5
[17] Djearamane S., Loh Z.C., Lee J.J. *et al*.: *Frontiers in Pharmacology* **2022**, *13*, 891304. https://doi.org/10.3389/fphar.2022.891304
[18] Ismail A.M., Menazea A.A., Kabary H.A. *et al*.: *Journal of Molecular Structure* **2019**, *1196*, 332. https://doi.org/10.1016/j.molstruc.2019.06.084
[19] Sudatta B.P., Sugumar V., Varma R. *et al*.: *International Journal of Biological Macromolecules* **2020**, *163*, 423. https://doi.org/10.1016/j.ijbiomac.2020.06.291
[20] Abu-Dalo M.A., Othman A.A., Al-Rawashdeh N.A.: *International Journal of Electrochemical Science* **2012**, *7*, 9303–9324. https://doi.org/10.1016/S1452-3981(23)16199-2
[21] Rao Y.N., Banerjee D., Datta A. *et al*.: *Radiation Physics and Chemistry* **2010**, *79(12)*, 1240. https://doi.org/10.1016/j.radphyschem.2010.07.004
[22] Devi P.G., Velu A.S.: *Journal of Theoretical and Applied Physics* **2016**, *10*, 233. https://doi.org/10.1007/s40094-016-0221-0
[23] Souza A.P., Neves J.G., Navarro da Rocha D. *et al*.: *Journal of Biomaterials Applications* **2023**, *37(9)*, 1605. https://doi.org/10.1177/08853282231155570
[24] Getie S., Belay A., Chandra Reddy A.R. *et al*.: *Journal of Nanomedicine and Nanotechnology* **2017**, *8*, 004. http://dx.doi.org/10.4172/2157-7439.S7-001
[25] Jobe M.C., Mthiyane D.M., Mwanza M. *et al*.: *Heliyon* **2022**, *8(12)*, e12243. https://doi.org/10.1016/j.heliyon.2022.e12243
[26] Bharathi D., Ranjithkumar R., Chandarshekar B. *et al*.: *International Journal of Biological Macromolecules* **2019**, *129*, 989. https://doi.org/10.1016/j.ijbiomac.2019.02.061
[27] Rodríguez-Rodríguez R., Velasquillo-Martínez C., Knauth P. *et al*.: *Journal of Biomedical Materials Research Part A* **2020**, *108*, 81. https://doi.org/10.1002/jbm.a.36794
[28] Abdeen Z.I., El Farargy A.F., Negm N.A.: *Journal of Molecular Liquids* **2018**, *250*, 335. https://doi.org/10.1016/j.molliq.2017.12.032
[29] Mostafa M.H., Elsawy M.A., Darwish M.S. *et al*.: *Materials Chemistry and Physics* **2020**, *248*, 122914. https://doi.org/10.1016/j.matchemphys.2020.122914

Received 29 II 2024.
Accepted 24 IV 2024.

Rapid Communications

Przypominamy Autorom, że publikujemy artykuły typu **Rapid Communications – prace oryginalne wyłącznie w języku angielskim** (o objętości 4–5 stron maszynopisu z podwójną interlinią, zawierające 2–3 rysunki lub 1–2 tabele), którym umożliwiamy szybką ścieżkę druku (do 3 miesięcy od chwili ich otrzymania przez Redakcję). Artykuł należy przygotować wg wymagań redakcyjnych zamieszczonych we wskazówkach dla P.T. Autorów.

* * *

We remind Authors that we publish articles of the **Rapid Communications** type – **the original papers, in English only** (with a volume of 4-5 pages of double-spaced typescript, containing 2–3 figures or 1–2 tables), which allow a fast print path (up to 3 months from when they are received by the Editorial Board). The article should be prepared according to the editorial requirements included in the Guide for Authors.